Journal of Applied Sciences 5 (1): 162-168, 2005
ISSN 1607-8926

Improvement of the Magnetic Properties of Mn-Ni-Zn Ferrite by the Non-magnetic Al^{3+}-Ion Substitution

[1]A.A. Sattar, [1]H.M. El-Sayed, [2]K.M. El-Shokrofy and [2]M.M. El-Tabey
[1]Department of Physics, Faculty of Science, Ain Shams University, 11566 Abbassia, Cairo, Egypt
[2]Department of Physics and Mathematical Engineering, Faculty of Engineering,
Menoufia University, Shebin El-Kom, Egypt

Abstract: The effect of Al-substitution on the physical, IR spectra and magnetic properties of $Mn_{0.5}Ni_{0.1}Zn_{0.4}Al_xFe_{2-x}O_4$ (x=0 to x=0.15, with step= 0.025) ferrites, prepared by conventional ceramic method, has been studied. The analysis of IR spectrum indicated the distribution of Al-ions between both A and B-sites. On Al substitution, the values of saturation magnetization, initial permeability and Curie temperature were increased. The dc resistivity is also increased with increasing Al-content. Such results are promising ones for the high frequency applications.

Key words: Ferrites, IR-spectra, magnetic properties, Mn-Ni-Zn ferrites, Al^{3+}-substituted ferrites

INTRODUCTION

From the applications point of view, both Mn-Zn and Ni-Zn ferrites represent the most important types where they are used in many ferrite devices such as inductor cores, converters, magnetic heads, electromagnetic wave absorbers etc. Mn-Zn ferrites possess high initial permeability and magnetization but these ferrites are not suitable for magnetic applications at high frequency due to their high electrical conductivity and therefore high power losses. Ni-Zn ferrites, on the other hand, have high resistivity, low-dielectric loss and high Curie temperature but they have relatively low initial permeability at high frequencies. Recently many authors studied the combination of these two ferrites in order to obtain favorable magnetic properties with low losses especially at high frequencies. The microstructure, the magnetic properties and the dc resistivity of $Mn_xNi_{0.5-x}Zn_{0.5}Fe_2O_4$ ferrites, prepared by citrate precursor method, has been investigated[1,2]. Unfortunately, the resistivity decreased with increasing Mn-content. The effect of sintering and microstructure on the initial permeability for $Mn_{0.02}Ni_{0.68}Zn_{0.25}Fe_{2.05}O_4$ and $Mn_{0.2}Ni_{0.2}Zn_{0.6}Fe_2O_4$ were studied[3,4]. It was found that, the sintering temperature has a great effect on the structural and magnetic properties of these ferrites. Finally, the Mn-substitution effect on the conductivity, magnetic properties and dielectric behavior of Ni-Zn ferrites was carried out[5,6]. It was found that, there was an enhancement in the saturation magnetization. However, the initial permeability, Curie temperature and dc resistivity were decreased with increasing Mn-content. In the present study, the effect of Al-substitution on the physical, IR spectra, the magnetic properties and electrical resistivity of $Mn_{0.5}Ni_{0.1}Zn_{0.4}Al_xFe_{2-x}O_4$ ferrites will be studied.

MATERIALS AND METHODS

Ferrite samples with chemical formula $Mn_{0.5}Ni_{0.1}Zn_{0.4}Al_xFe_{2-x}O_4$ (x=0 to x=0.15, with step 0.025) were prepared by conventional ceramic method. High purity oxides, 99.99%, of NiO, ZnO, Al_2O_3 and Fe_2O_3 with $MnCO_3$ were mixed together according to their molecular weights. The mixture of each composition was ground to a very fine powder and presintered at 900°C for 15 h. The presintered mixture was ground again and pressed at room temperature under a pressure of 3.8×10^8 Pa into tablet and toroidal forms. They were finally sintered at 1300°C for 4 h in two cycles and then slowly cooled in N_2 atmosphere to room temperature at a rate of 1°C/min.

X-ray diffraction patterns were performed using a diffractometer of type X`Pert Graphics and identify with Cu $K_\alpha$ radiation. The theoretical X-ray density ($d_x$) of the samples was calculated using the formula ($d_x=8M/Na^3$) where, M is the molecular weight, N is Avogadro`s number and a is the lattice parameter. The density d of each composition was measured in toluene using Archimedes principle. The porosity percentage P(%) was calculated according to the relation $P=100\ [1-(d/d_x)]$ %. The FTIR spectra were carried out (using Perkin Elmer

Corresponding Author: A.A. Sattar, Department of Physics, Faculty of Science, Ain Shams University, 11566 Abbassia, Cairo, Egypt E-mail: Adel_Sattar@hotmail.com

specto-photometer) in the range from 200-600 cm^{-1}. The grain size was obtained by scanning electron microscope (SEM) type (JEOL JSM5600). The magnetization (M_S) was measured using the vibrating sample technique. The magnetizing field ranges from 0.0 up to 1 Tesla. Toroidal shaped samples of inner diameter = 0.75 cm, outer diameter = 1.55 cm and average thickness ~0.3 cm were used as transformer cores for measuring the initial permeability. The initial permeability μ_i was measured as a function of temperature at a constant frequency f = 10 KHz of a sinusoidal wave. The magnetizing current in the primary coil I_p is kept constant at 4 mA. The value of μ_i was calculated using Poltinnikov`s formula[7]. According to this formula we have, $V_S=K\,\mu_i$ where, V_S is the induced voltage in the secondary coil and $K=0.4\Pi\, I_P N_P N_S A\omega/L$ where, N_P and N_S are the number of turns of primary and secondary coils, respectively ($N_P = N_S = 15$ turn), A is the cross-section area of the sample, ω is the angular frequency and L is the average path of the magnetic flux.

RESULTS AND DISCUSSION

Physical properties

X-ray analysis: The formation of single phase of $Mn_{0.5}Ni_{0.1}Zn_{0.4}Al_xFe_{2-x}O_4$ ferrites is concluded from the XRD patterns of the investigated samples. The values of lattice parameters are determined using Bragg's law and are plotted as a function of Al-ion concentration in Fig. 1. It is clear that as the Al-concentration increases, the lattice parameter decreases. Similar behavior was observed in Al-substituted both Mn-Zn[8-10] and Ni-Zn ferrites[11]. The decrease in lattice parameter with Al-concentration could be easily explained on the basis of the ionic radii where the radius of Al-ion (≈0.51Å) is smaller than that of the iron ion (≈0.67Å).

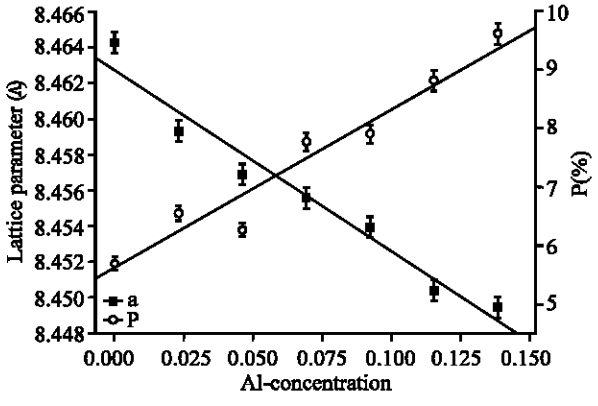

Fig. 1: The variation of the lattice parameter a (Å) and porosity P(%) with Al-Concentration(x)

For the spinel structure, the theoretical lattice parameters a_{th} could be calculated using the following equation[12]:

$$a_{th} = \frac{8}{3\sqrt{3}}\left[(r_A + r_O) + \sqrt{3}\,(r_B + r_O)\right] \quad (1)$$

where, r_o is the radius of the oxygen ion (1.32 Å), r_A and r_B are the ionic radii of tetrahedral (A-site) and octahedral (B-site) sites, respectively. To calculate r_A and r_B, the following cation distribution is assumed;

$$(Al_t^{3+}Zn_{0.4}^{2+}Fe_{0.2}^{3+}Mn_{0.4-t}^{2+})$$

$$[Al_{x-t}^{3+}Mn_{0.1+t}^{2+}Ni_{0.1}^{2+}Fe_{1.8-x-y}^{3+}Fe_y^{2+}]O_4 \quad (2)$$

This cation distribution is based on the following:

1. For the unsubstituted sample, 80% of Mn-ions occupy the tetrahedral position (A-site) and the remaining, 20%, occupy the octahedral position (B-site)[13]. For substituted samples, this ratio is slightly changed due to Al-substitution.
2. Zn ions prefer to occupy the tetrahedral sites while Ni ions occupy the octahedral sites.
3. Concerning Al^{3+}-ion distribution, there are two points of views. The first one is that the Al^{3+}-ions in spinel ferrites are distributed on both tetrahedral and octahedral sites, such that, the majority of Al-ions occupy the octahedral position[14-20]. The other one is that the Al^{3+}-ions occupy completely B-sites[11,21-23]. IR spectroscopic analysis, as it will be discussed later, shows that Al ions are distributed on both A and B-sites.

In this cation distribution, the formation of Fe^{2+}-ion during the sintering process is taken into consideration. The ionic radius for each site is calculated according to the following equations:

$$r_A = (t\,r_{Al^{3+}} + 0.4\,r_{Zn^{2+}} + 0.2\,r_{Fe^{3+}} + (0.4-t)\,r_{Mn^{2+}})$$

$$r_B = \frac{1}{2}\left[(x-t)\,r_{Al^{3+}} + (0.1+t)\,r_{Mn^{2+}} + (1.8-x-y)\,r_{Fe^{3+}} + y\,r_{Fe^{2+}}\right.$$

where, r_{AL3+}, r_{Zn2+}, r_{Mn2+}, r_{Fe3+} r_{Ni2+} and r_{Fe2+} are the ionic radii of aluminum, zinc, manganese, trivalent iron ion, nickel and divalent iron ion, respectively. The values of the ionic shows that the ionic radius depends on the coordination number[24]. The values of t and y in the assumed cation distribution, were chosen as fitting parameters such that good fitting between a_{Th} and $a_{Exp.}$ is obtained (Table 1).

Porosity and grain size: Figure 1 also shows that, as Al-content increases the porosity P(%) increases. It is

Table 1: The values of t and y with Al-concentration

Al-Conc. (x)	(t)	Fe^{2+}-Conc. (y)
0.000	0.000	0.180
0.025	0.012	0.170
0.050	0.020	0.162
0.075	0.024	0.155
0.100	0.030	0.146
0.125	0.037	0.126
0.150	0.040	0.114

known that, the porosity of ceramic samples results from two sources, intragranular porosity (P_{intra}) and intergranular porosity (P_{inter})[25]. Thus the total porosity P(%) could be written as the sum of the two types i.e.,

$$P(\%) = (P_{intra} + P_{inter}) \quad (3)$$

Furthermore, it was reported that the intergranular porosity (P_{inter}) depends on the grain size[9,25]. By studying the scanning electron microscope (SEM) for the samples, it is found that as the Al-concentration increases from x =0.05 up to x=0.15 there is no considerable change in the grain size. Therefore as Al-content increases the intergranular porosity (P_{inter}) remains almost constant. Thus according to equation (3), the increase of the total porosity P(%) results mainly from the increase of intragranular porosity (P_{intra}) with Al-concentration. Such a conclusion is in agreement with that previously reported in case of Al-substituted of Zn and Cu-Cd ferrites[10,21].

IR-spectral analysis: The study of far-infrared spectrum is an important tool to get information about the positions of the ions in the crystal through the crystal's vibrational modes[26]. It is known that the normal and inverse cubic spinels have four IR bands representing the four fundamentals {υ_1, υ_2, υ_3 and υ_4}[27]. It has been reported that, the first three IR fundamental bands are due to tetrahedral and octahedral complexes, while the fourth one is due to the lattice vibrations[26]. Figure 2 shows the IR spectra of some studied samples (x = 0.0, 0.05, 0.1 and 0.15). The positions of their bands are given in Table 2. The high frequency bands υ_1 (547-561) and υ_2 (378-409) are attributed to the vibration of iron ions in both tetrahedral and octahedral positions, respectively. The third vibrational frequency band υ_3 (310-344) is associated with the divalent octahedral metal ions and oxygen complexes. Finally, the fourth vibrational band (υ_4) (220-288) is attributed to the lattice vibrational frequency[28].

It is obvious from the Table 2 that as Al-concentration (x) increases υ_1 shifts to higher frequency while υ_2 shifts to lower frequency. These shifts in the frequencies of the bands could be explained on the basis that the change in the bond length has an inverse relation with the band frequency shift[8]. Figure 3 shows

Table 2: Frequency (cm^{-1}) of the IR observed bands

Al-Conc.	Tetra.	Octahedral bands			Lattice vibration		
(x)	υ_1	υ_2	υ_3		υ_4		
0.00	547	409	344	324	272	240	222
0.05	553	398	348	319	277	249	221
0.10	559	397	343	307	278	248	220
0.15	561	378	344	310	288	240	222

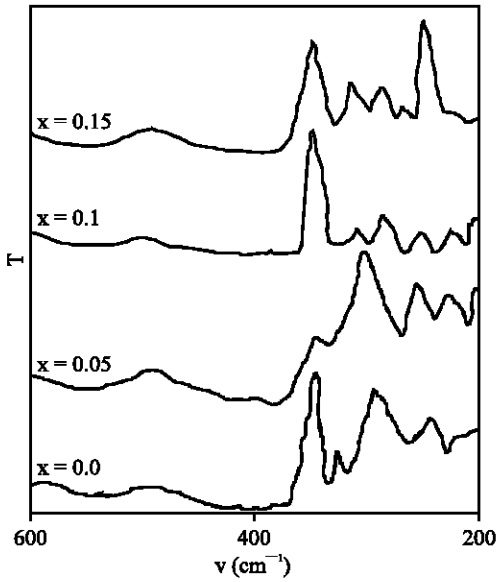

Fig. 2: IR-spectrum of samples with x=0.0, 0.05, 0.10 and 0.15

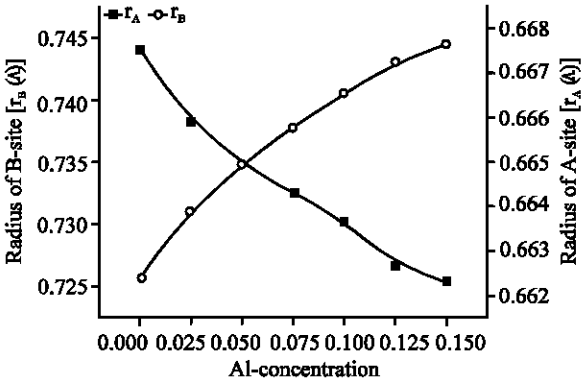

Fig. 3: Variation of tetrahedral (r_A) and octahedral (r_B) radii with Al-content

the variation of the radii of tetrahedral site (r_A) and octahedral site (r_B) with Al-content. It is clear that as Al-concentration increases, r_A decreases while r_B increases, which explain the increase of υ_1 and the decrease of υ_2 and υ_3. The shift of the lattice vibration band υ_4 to the higher frequency could be attributed to the difference in masses between the substituted and displaced ions. In this composition, Fe^{3+}-ions are replaced

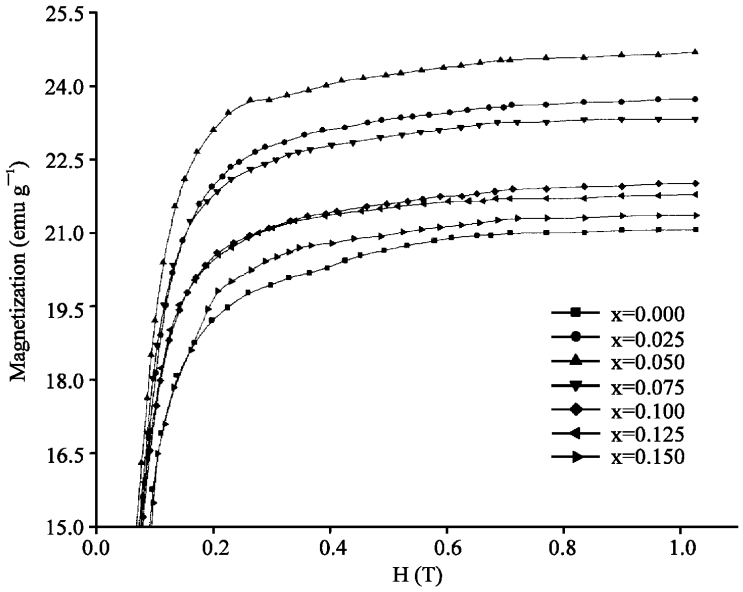

Fig. 4: The magnetization M (emu g^{-1}) versus the applied magnetic field H (T)

by Al^{3+}-ions which have smaller mass than that of Fe^{3+}. Thus, the total mass of lattice decreases leading to an increase of the frequency band υ_4.

Magnetic properties

Magnetization and coercive field: The variation of magnetization M (emu g^{-1}) with the static applied magnetic field H (up to 1 Tesla) for all investigated samples at room temperature is shown in Fig. 4. As a normal behavior, the magnetization increases with increasing the applied magnetic field and attains its saturation value for fields higher than 0.6 Tesla. The dependence of saturation magnetization M_s, determined by extrapolation of the magnetization curve to H=0, on the Al-concentration (x) is shown in Fig. 5. It is clear that, as the Al-ion concentration increases M_s increases rapidly to have a maximum value at x=0.05 and then it decreases with increasing the Al-concentration. This behavior could be explained according to the above assumed cation distribution. It is known that, for Mn-Zn and Ni-Zn ferrites there is a canting angel, Yafet-Kittel angle (α_{YK}), between the moments in B-site at Zn-concentration ≈0.4. Such a canting is due to the negative B-B interaction[29,30]. Thus the total magnetization M could be expressed as[21]

$$M = M_B \cos \alpha_{YK} - M_A \qquad (4)$$

where, M_A and M_B are the magnetic moments of A and B-sites, respectively. Using the assumed cation distribution and taking the values of the magnetic moments of Fe^{3+}, Fe^{2+}, Zn^{2+}, Ni^{2+},Al^{3+} and Mn^{2+}as 5, 4, 0, 2, 0 and 5 μ_B, respectively, the total magnetic moment is written as;

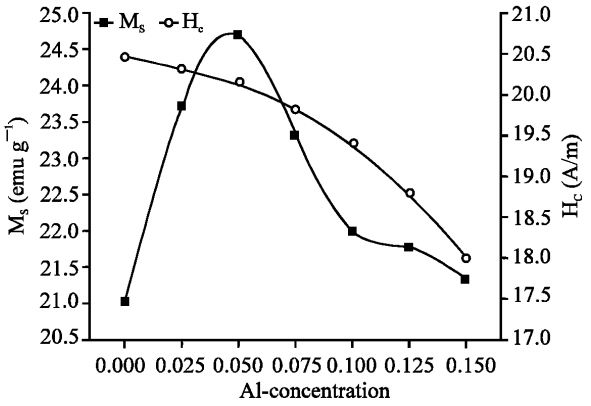

Fig. 5: The variation of saturation magnetization M_s (emu g^{-1}) and coercive Field H_c (A m^{-1}) with Al-concentration

$$M = \mu_B (9.8-5x+5t-y) \cos \alpha_{YK} + (5t-3) \mu_B \qquad (5)$$

In view of equation (5) and according to the values of x and t, in Table 1, the increase of M with x up to x=0.05 can be attributed to the increase of $\cos\alpha_{YK}$ i.e. a decrease of α_{YK}. For x>0.05, i.e. further replacement of Fe^{3+} ions by non magnetic Al^{3+} ions in B-sites, leads to a decrease of the magnetization of the B-sites and hence the total magnetization should decrease as we found experimentally. In other words, after improving the parallelism at x=0.05, further replacement of Fe^{3+}ions by

non-magnetic Al^{3+} ions in B-site leads to decrease the value of M_B and hence the total magnetization M should decrease.

The percentage increase in saturation magnetization ($\Delta M_S\%$) of the Al-substituted samples is listed in Table 3.

It is clear that, for Al-concentration x=0.05, the percentage increase of M_S, at room temperature, reaches to about 17% greater than that of un-substituted one which is an important result from the technological point of view.

Figure 5 shows the change of the coercive filed (H_c) with Al-concentration (x) at a magnetizing field H=300 A m^{-1}. It is obvious that Hc decreases with increasing Al-content. This behavior could be explained through Brown's relation[31] which is given by:

$$H_C \geq \frac{2K_1}{\mu_O M_S} \quad (6)$$

where, K_1 is the anisotropy constant. It is known that the anisotropy field in ferrites results mainly from the presence of Fe^{2+} ions[32]. According to the above results, for x=0.05, K_1 decreases (the concentration of Fe^{2+} ions decreases) while M_S increases. Thus the two factors enhance the decrease of H_C. For x> 0.05, both K_1 and M_S decrease with increasing Al concentration. Thus the decrease of H_C for high Al concentration indicates that K_1 is the dominant factor. The decrease of K_1 due to Al-substitution in different ferrites was previously reported[10,21].

Table 3: The values of M_S, $\Delta M_S\%$, μ_i and $\Delta\mu_i$ (%) at room temperature

Al-conc. (x)	M_S (emu g^{-1})	ΔM_S (%)	μ_i	$\Delta\mu_i$ (%)
0.000	21.03	---	223.3	---
0.025	23.71	12.77	331.6	48.5
0.050	24.68	17.34	367.9	64.7
0.075	23.31	10.84	288.5	29.2
0.100	21.99	4.578	287.8	28.9
0.125	21.76	3.493	296.2	32.6
0.150	21.33	1.419	296.6	32.8

Initial permeability and curie temperature: Figure 6 shows the variation of the initial permeability μ_i with temperature T(K) for all samples. It is found that the curves are typical of multidomain grains showing a sudden drop in μ_i at T_C. The Curie temperature T_C is determined by drawing a tangent for the curve at the rapid decrease of μ_i. The intersection of the tangent with the T-axis determines T_C. The dependence of both initial permeability μ_i at room temperature and T_C on the Al-concentration are shown in Fig. 7. It is obvious that, μ_i follows the same behavior as that of M_S where a maximum is noticed at x=0.05. The similarity in behavior of μ_i and M_S with Al-concentration x arises directly from the approximate equation for the initial permeability[33].

$$\mu_i \cong (M_S^2 D/\sqrt{K_1}) \quad (7)$$

where, D is the average grain diameter. The percentage increase of the initial permeability $\Delta\mu_i(\%)$ for the Al-substituted samples are reported in Table 3. The values of ($\Delta\mu_i\%$) are in the range (29-64%). It is also

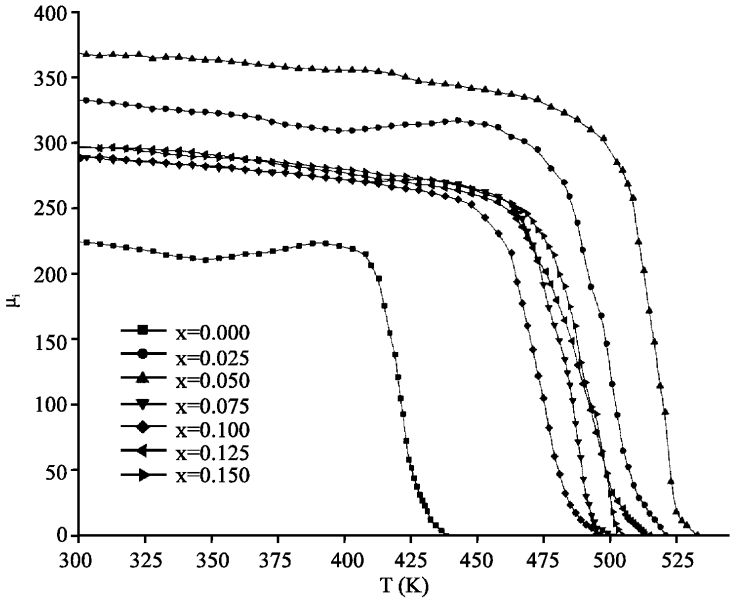

Fig. 6: The temperature dependence of the initial permeability μ_i for different Al concentration

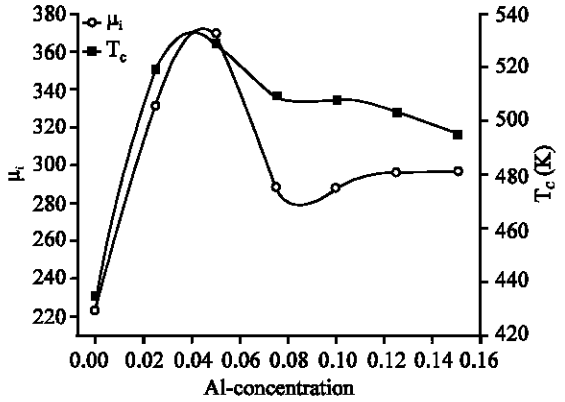

Fig. 7: The variation of the initial permeability μ_i (at room temperature) and Curie temperature T_c(K) with the Al-concentration

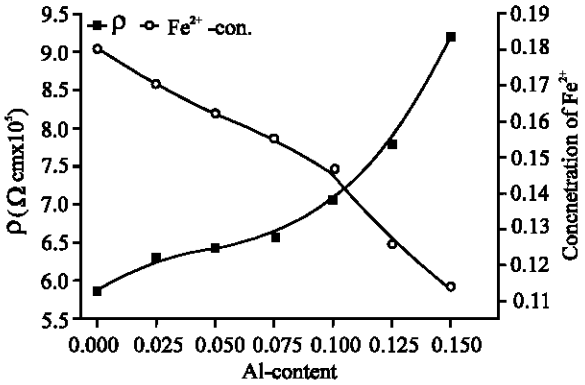

Fig. 8: The dependence of the electrical resistivity ρ (at room temperature) and Fe^{2+} ion concentration on the Al-content

observed that the values of T_C for all substituted samples are greater than that of un-substituted one. This could be attributed to the decrease in the distance between the moments of A and B-sites which is confirmed by the decrease in the lattice parameter with Al-content. The shortage in distances between moments leads the A-B interaction to increase for substituted samples relative to un-substituted one and consequently the T_C is increased.

Resistivity at room temperature: The dependence of electrical resistivity (ρ), at room temperature and the concentration of Fe^{2+}-ion on the Al-content is shown in Fig. 8. It is clear that the substitution of Al ion leads to increase the resistivity. The increase of ρ is attributed to two factors:

1. the decrease of Fe^{2+}-ion concentration which limits the hopping probability between Fe^{3+} and Fe^{2+}-ions.
2. The increase of the intragranular porosity which in turn hinders the motion of charge carriers.

CONCLUSION

- The lattice parameter decreases while the porosity increases with Al-ion substitution in Mn-Ni-Zn ferrites.
- The IR-analysis supports the distribution of Al-ions in both A and B sites.
- Al-ion substitution improves both the saturation magnetization and initial permeability.
- Curie temperatures and the dc resistivity of Mn-Ni-Zn ferrites are increased for all substituted samples. These results are promising in high frequency applications.

REFERENCES

1. Amarendra, K.S., T.C. Goel and R.G. Mendiratta, 2002. Magnetic properties of Mn-substituted Ni-Zn ferrites. J. Applied Phys., 92: 3872-3876.
2. Amarendra, K.S., A.Verma, O.P. Thakur, C. Prakash, T.C. Goel and R.G. Mendiratta, 2002. DC Resistivity of Mn-Ni-Zn Ferrites. Jpn. J. Applied Phys., 41: 5142-5144.
3. Japes, B., K.S. Ashim and M. Aravind, 2000. Sintering and surfase microstructure of Ni-Zn ferrites. Proc. (ICF 8), Kyoto and Tokyo, Japan, pp: 536-538.
4. Amarendra, K.S., T.C. Goel and R.G. Mendiratta, 2004. Low-temperature synthesis of $Mn_{0.2}Ni_{0.2}Zn_{0.6}Fe_2O_4$ ferrites by citrate precursor method and study of their properties. Phys. Stat. Sol., 201: 1453-1457.
5. Amarendra, K.S., T.C. Goel and R.G. Mendiratta, 2003. Effect of manganese impurity on the conductivity, Dielectric behavior and magnetic properties of $Ni_{0.3}Mn_xZn_{0.7-x}Fe_2O_4$. Jpn. J. Applied Phys., 42: 2690-2691.
6. Rezlescu, E., L. Sachelarie, P.D. Popa and N. Rezlescu, 2000. Effect of substitution of divalent ions on the electrical and magnetic properties of Ni-Zn-Me Ferrites. IEEE Trans. Magnet, 36: 3962-3967.
7. Poltinnikov, S.A.J, 1966. Some magnetic properties of nickel-cadmium ferrite. Sov. Phys. Solid Stat., 8: 1144-1149.
8. Chandrasekaran, G., S. Selvandan and K. Manivannane, 2004. Electrical and FTIR studies on Al substituted Mn-Zn mixed ferrites. J. Mate. Sci.: Materials in Electronics, 15: 15-18.
9. Rezlescu, N., E. Rezlescu, C. Pasnicu and M.L. Craus, 1994. Effect of the rare-earth ions on some properties of a nickel-zinc ferrite. J. Phys. Condens. Matter, 6: 5707.

10. Kakatkar, S.V., S.S. Kakatkar, R.S. Patil, P.K. Maskar, A.M. Sankapal, S.S. Suryawanshi, N.D. Chaudhari and S.R. Sawant, 1996. X-ray and bulk magnetic properties of aluminium substituted ferrites. J. Mag. Mate., 159: 361-366.
11. Chandra, P., 1987. Effect of aluminium substitution on electrical conductivity and physical properties of zinc ferrite. J. Mate. Sci. Lett., 6: 651-652.
12. Mazen, S.A., M.H. Abdallah, B.A. Sabrah and H.A.M. Hashem, 1992. The Effect of titanium on some physical properties of $CuFe_2O_4$. Phys. Stat. Sol., 134: 263-271.
13. Petil, F. and M. Lenglet, 1993. Spectroscopic evidence of the Mn^{3+}-Fe^{2+} octahedral pair in lithium-manganese ferrites near the order-disorder transition. Solid State Communications, 86: 67.
14. AboElAta, A.M., S.M. Attia and T.M. Meaz, 2004. AC conductivity and dielectric behavior of $CoAl_xFe_{2-x}O_4$. J. Solid State Sci., 6: 61-69.
15. Urvi, V., S. Bimal and R. Kulkarni, 1999. Magnetic properties of the mixed spinel Ni $Al_{2x}Cr_xFe_{2-3x}O_4$. Physica B., 262: 5-12.
16. Seo Wook, Young Lee, Kwang Pyo and Sungtto, 1999. Mossbauer study of the Cu_{1-x} Mn_x $Fe_{2-y}Al_yO_4$ system. J. Korean Phy. Soc., 34: 378-384.
17. Kulkarni, R.G., S. Bimal and G. Baldha, 1996. Magnetic properties of copper ferrite aluminates. J. Mag. Mate., 159: 375-380.
18. Jung, T., D. Park and S. Kwon, 1995. Ion distribution and saturation magnetization of aluminum substituted lithium ferrites. IEEE. Trans. Magnet, 31: 3979-3981.
19. Ashfaq, A., 1992. Investigation of structural transport and magnetic properties of the system $Li_{0.25}Cu_{0.5}Fe_{2.25-x}Al_xO_4$. J. Mate. Sci., 27: 4120-4124.
20. Rosenberg, M., P. Deppe and H. Janssen, 1985. A Mossbauer study of Al and Ga substituted magnetite. J. Applied Phys., 57: 3740-3742.
21. Suryawanshi, S.S., V. Deshpand and S.R. Sawant, 1999. XRD analysis and bulk magnetic properties of Al^{3+} substituted Cu-Cd ferrites. J. Mate. Chem. Phys., 59: 199-203.
22. Sankpal, A.M., S.V. Kakatkar and S.R. Sawant, 1998. Initial permeability studies on Al^{3+} and Cr^{3+} substituted Ni-Zn ferrites. J. Mate. Sci.: Materials in Electronics, 9: 173-179.
23. Sparvieri, N. and N.P. Cattari, 1990. Influence of Al^{3+} substitution and sintering conditions on the properties of ceramic Mg-Mn microwave ferrites. J. Mate. Chem. Phys., 25: 167-175.
24. Shannon, R.D. and C.T. Prewitt, 1969. Effective ionic radii in oxides and fluorides. Acta Crystal, B., 25: 925-946
25. Kigery, W.D., H.K. Bowen, D.R. Uhlmann, 1975. Introduction of Ceramics Published by John Wiley and Sons New York, London, pp: 458.
26. Mohan, K and Venudhar, 1999. Far-infrared spectra of lithium-cobalt mixed ferrites. J. Mate. Sci. Lett., 18: 13-16.
27. Ravender, 1999. Far-infrared spectral studies of mixed lithium-zinc ferrites. J. Mate. Lett., 40: 205-208.
28. Ahmed, M.A, E. Ateia and S.I. El-dek, 2002. Spectroscopic analysis of ferrites doped with different rare earth elements. J. Vibrational Spectroscopy, 30: 69-75.
29. Kulkarini, R.G. and V.U. Patial, 1982. Magnetic Ordering In Cu-Zn Ferrite. J. Mate. Sci., 17: 843-848.
30. Chikazumi, S. and S. Charap, 1964. Physics of Magnetism. Published by John Wiley and Sons, Inc., New York, London, Sydney, pp: 93.
31. Coey, J.M.D., 1996. Rare-earth Permanent Magnetism. Published by John Wiley and Sons, New York, pp: 220.
32. Chikazumi, S. and S. Charap, 1964. Physics of Magnetism. Published by John Wiley and Sons, Inc., New York, London, Sydney, pp: 153.
33. Jain, G.C., B.K. Das, R.S. Khanduja and S.C. Gupta, 1976. Effect of intragranular porosity of initial permeability and coercive force in a manganese zinc ferrite. J. Mate. Sci., 11: 1335-1338.